A Nature Portfolio journal



https://doi.org/10.1038/s42003-025-08154-0

Monoacylglycerol acyltransferase maintains ionotropic receptor expression for cool temperature sensing and avoidance in *Drosophila*



Xiangmei Deng^{1,2}, Takuto Suito^{1,2,5}, Makoto Tominaga^{2,3} & Takaaki Sokabe © ^{1,2,4} 🖂

Sensory inputs of temperature dynamics in the environment are essential for appropriate physiological outputs. The responsiveness of sensory neurons is maintained by functional thermosensor expression. However, the mechanism by which their expression is regulated is unclear. In this study, we identify a monoacylglycerol acyltransferase-coding gene named *bishu-1* that contributes to maintaining the responsiveness of cool temperature sensing neurons in *Drosophila*. *bishu-1* mutation leads to abnormal thermal avoidance in a cool temperature range. Cooling-induced responses in dorsal organ cool cells are weakened by the absence of *bishu-1*, and this is associated with reduced transcription of the ionotropic receptors *IR25a* and *IR21a* and a transcription factor *broad*. Our findings unveil a novel link between lipid metabolism and thermosensor function, thus providing new insights into mechanisms underlying the appropriate maintenance of sensory inputs.

Environmental temperature is a critical parameter for all animals as they seek optimal habitats for survival and successful reproduction. To monitor surrounding temperatures, a wide range of species have evolved temperature sensing mechanisms involving thermosensitive molecules, including transient receptor potential (TRP) channels^{1,2}, other types of ion channels^{3,4}, and G protein-coupled receptors (GPCRs)⁵⁻⁸. Thermal sensation is particularly important for ectotherms such as insects because of their small body size and large surface-to-volume ratio, which leads to rapid core temperature fluctuation. Thus, their physiological functions, including long-term survival⁹, reproduction¹⁰, and diverse behavioral activities¹¹, are profoundly impacted by ambient temperature. To mitigate core temperature fluctuation, Drosophila has evolved a delicate thermosensory system that discriminates temperature changes within a millidegree per second¹². This accurate thermosensation relies on the precise maintenance of thermosensor functions. In addition to GPCRs and TRP channels^{5,7,13}, Drosophila larvae and adults use subsets of unique receptor families identified in invertebrates, such as ionotropic receptors (IRs) and a gustatory receptor for thermosensation¹⁴⁻¹⁸. However, the activation and regulatory mechanisms of many of these thermosensors remain to be clarified.

Lipids are important players in TRP channel regulation and sensory responses. For example, fatty acids serve as key signaling molecules that modulate TRP channels in multiple species¹⁹. In the aspect of thermosensory and regulatory behaviors in Drosophila, lipid products of phospholipase C β (PLCβ) signaling cascade and other membrane lipids have been reported; the thermal preference of larvae is influenced by desaturation and oxidization of membrane lipids²⁰⁻²². In adults, cold temperature activates bitter taste neurons expressing rhodopsin and PLC, which is essential for cold temperature-dependent feeding suppression²³. Low ambient temperature facilitates unsaturated fatty acid intake and egg laying on unsaturated fatty acid-containing food in adults²⁴, suggesting the importance of the saturation level of membrane lipids in the maintenance of biological functions. The PLC signaling cascade is also involved in other sensory processes of Drosophila. In phototransduction, products of PLC including diacylglycerol (DAG) and monoacylglycerol (MAG) activate TRP and TRPL channels^{25–27}. The same or related PLC products possibly regulate TRPA1 in taste neurons in response to bitter compounds²⁸. These facts suggest that diacylglycerol and relevant metabolites in PLC and other signaling cascades are key components for receptor and sensory functions. However, the regulatory mechanisms and physiological importance of associated lipid enzymes in thermosensory processes have not been thoroughly clarified.

Transcriptional regulation of sensors by lipids is one possible mechanism to maintain receptor function. In support of this, accumulated

¹Thermal Biology Group, Exploratory Research Center on Life and Living Systems, National Institutes of Natural Sciences, Okazaki, Japan. ²Section of Sensory Physiology, Center for Genetic Analysis of Behavior, National Institute for Physiological Sciences, National Institutes of Natural Sciences, Okazaki, Japan. ³Thermal Biology Research Group, Nagoya Advanced Research and Development Center, Nagoya City University, Nagoya, Japan. ⁴Graduate Institute for Advanced Studies, SOKENDAI, Hayama, Japan. ⁵Present address: Ezaki Glico Co., Ltd., Osaka, Japan. ⊠e-mail: sokabe@nips.ac.jp

evidence links lipids and transcription. For example, polyunsaturated fatty acids function as ligands of nuclear receptors such as peroxisome proliferator-activated receptor (PPAR) and the transcription factor sterol regulatory element binding protein (SREBP) in multiple tissues in mammals^{29,30}. DAG is an activator of protein kinase C (PKC), which is coupled with the activation of multiple transcription factors such as Nuclear factor-kappa B (NFKB), activator protein 1 (AP-1)³¹, signal transducers and activators of transcription 3 (Stat3)³², and c-Rel³³. Additionally, a recent report suggested that the activity of the Max-like protein X (MLX) family of transcription factors is suppressed through binding to lipid droplets, which are formed by DAG and acylglycerol acyltransferases³⁴. However, whether DAG affects transcription in neurons remains unknown.

In this study, we conducted thermotaxis screenings using Drosophila larvae and identified two DAG synthesis genes, namely bishu-1 and bishu-2. The name "bishu" given to the gene is a Chinese word for "summering", describing the escaping behavior of larvae from heat. bishu-1 and bishu-2 mutations led to defects in cool temperature avoidance. These genes formed a cluster on the genome, and their amino acid sequences were close to those of the human diacylglycerol acyltransferase 2 (DGAT2) family. bishu-1 and bishu-2 were distinctly expressed in multiple sensory neurons to regulate thermal preference, and bishu-1 particularly functioned in cool temperature-sensitive dorsal organ cool cells (DOCCs) expressing a set of thermosensors IR21a, IR25a, and IR93a. The abnormal cool temperature avoidance in bishu-1^{KO} was sufficiently rescued by human monoacylglycerol acyltransferase (MGAT) genes, suggesting the importance of their conserved function as acyltransferases in thermosensation. In vivo GCaMP imaging revealed that the response of DOCCs to cool temperature was diminished in the bishu-1^{KO}. The reduced responses of bishu-1^{KO} DOCCs were attributed to the downregulation of IR21a and IR25a mediated by the transcription factor broad (br). These results unveil a novel mechanism by which lipid metabolism regulates receptor function in sensory neurons through maintaining gene expression.

Results

Putative acylglycerol acyltransferases are involved in cool temperature avoidance

Based on previous studies identifying the involvement of the phospholipase C (PLC) pathway in thermosensation²⁰ with DAG as a key metabolite, we examined thermal preference in Drosophila strains with mutations in 12 genes encoding enzymes potentially involved in DAG metabolism. P-element insertion lines targeting phospholipase A genes and putative genes involved in anandamide metabolism exhibited no clear alterations in thermal gradient distribution patterns. In contrast, mutants of multiple genes, potentially implicated in DAG metabolism, showed tendencies of leftward or rightward shifts in distribution relative to controls. From these candidates, we selected a putative acylglycerol acyltransferase CG1942/ bishu-1 for further clarification. Genomic analysis revealed that bishu-1 forms part of a tandem gene cluster with two structurally homologous genes, CG1941 and CG1946/bishu-2 (Supplementary Fig. 1A). Phylogenetic analysis with amino acid sequences from human DGAT1 and DGAT2 families indicated that proteins encoded by CG1941, bishu-1, and bishu-2 have a closer evolutionary relationship with human DGAT2 family (Fig. 1A). This family contains MGATs, DGATs, and acyl-CoA wax alcohol acyltransferase (AWATs). Among all, Bishu-1 displayed higher amino acid identity with MGATs (MGAT2: 39.5%, MGAT3: 38.1%, MGAT1: 35.5%) than other members (DGAT2: 30.7%, AWAT1 35.1%). Because human MGATs produce DAG using acyl-CoA and MAG as substrates^{35–37}, we predicted bishu-1 as a DAG synthesis enzyme-coding gene. To study the effect of loss of function of each gene on thermal preference, we generated knockout lines of CG1941, bishu-1, and bishu-2 using the CRISPR-Cas9 technique. CG1941^{KO} was generated by introducing a deletion in the first exon to induce a frameshift (Supplementary Fig. 1B, top), whereas bishu-1^{KO} and bishu-2^{KO} were generated by inserting a *DsRed* reporter downstream of the start codon to interrupt their expression (Supplementary Fig. S1B, middle and bottom). The mRNA level of the target gene was abolished in each allele, indicating they were null mutants (Supplementary Fig. 1C). The mRNA level of a neighboring gene in each knockout was reduced by approximately 50% despite the lack of a mutation in its coding sequence, suggesting that the expression of each gene is maintained reciprocally (Supplementary Fig. 1C).

We tested the thermal preference of these knockouts on a linear temperature gradient of 8-35 °C (Fig. 1B), covering optimal and noxious temperature ranges. We released the cohort of early third instar larvae [72 h after egg laying (AEL)] at 23 °C and allowed them to explore the thermal landscape on the plate under a dim red light (>600 nm). Control larvae most accumulated in the 23–26 °C zone (32.5% \pm 3.8%, Fig. 1C; 33.6% \pm 5.7%, Fig. 1D). Their preferred temperature, which is the median staying temperature of larvae on the gradient, was approximately 24 °C [24.2 °C \pm 0.5 °C (left) and 24.1 °C ± 0.4 °C (right), Fig. 1E], which was consistent with previous studies^{7,38}. The thermal preference of CG1941^{KO} was comparable to that of the control, with the largest population in the 23-26 °C zone $(38.5\% \pm 2.7\%$, Supplementary Fig. 1D), and the preferred temperature was 23.4 °C \pm 0.3 °C. By contrast, bishu-1^{KO} and bishu-2^{KO} tended to distribute in a cooler range (11-20 °C) with the largest population in the 20-23 °C zone $(31.7\% \pm 4.3\% \text{ in } bishu-1^{KO} \text{ and } 24.2\% \pm 2.2\% \text{ in } bishu-2^{KO}, \text{ Fig. 1C, D)}$. The preferred temperatures of bishu-1^{KO} and bishu-2^{KO} were significantly reduced to 21.3 °C \pm 0.7 °C and 20.0 °C \pm 0.8 °C, respectively (Fig. 1E). On the other hand, the control and all three knockouts consistently avoided the lowest temperature zone (8-11 °C). The defect in cool temperature avoidance by bishu-1^{KO} and bishu-2^{KO} was rescued by introducing a genomic insertion containing the wild-type alleles of bishu-1 and bishu-2 (Fig. 1C-E). These results suggest that the putative acylglycerol acyltransferases are specifically involved in the avoidance of innocuous cool temperatures.

Because Drosophila melanogaster larvae display a developmentdependent switch in thermal preference from warm to cool temperatures^{7,38}, we evaluated the developmental rate of the control and the knockouts. The proportion of third instar stage at 74 h AEL and the pupation timing did not differ among the genotypes (Supplementary Fig. 1E, F). We observed that bishu-1^{KO} and bishu-2^{KO} displayed a less visible shift in distribution to cooler ranges on the thermal gradient both at the second (48 h AEL, Supplementary Fig. 1G) and late third instar stages (120 h AEL, Supplementary Fig. 1H) compared to the early third instar stage (72 h AEL, Fig. 1C, D). The bishu-1^{KO} and bishu-2^{KO} phenotypes at 120 h AEL may be influenced by the development-dependent switch of thermal preference through the rhodopsin pathway⁷ and IR expression changes³⁸. The mild phenotypes observed at 48 h AEL are likely caused by stronger inherent bias toward the 23-26 °C zone compared to 72 h AEL³⁹ (Fig. 1C, D, Supplementary Fig. 1G) through an unidentified mechanism independent of bishu-1 and bishu-2.

To further confirm that cool temperature avoidance depends on bishu-1 and bishu-2, we conducted a thermal two-way choice assay (Fig. 1F). Based on the preferred temperature of the early third instar control larvae on the thermal gradient (Fig. 1E), we set 24 °C as a reference against the test temperatures. We released larvae at a border of 24 °C and test temperature between 16 °C and 28 °C with a 2 °C interval and allowed them to choose two temperature zones. We counted the number of larvae on each side and calculated the preference index (PI). We observed that control and CG1941^{KO} larvae preferred 24 °C to cooler or warmer testing temperatures (Supplementary Fig. 1I), which was consistent with the gradient assay results and previous studies^{7,38}. bishu-1^{KO} and bishu-2^{KO} avoided temperatures exceeding 24 °C, similar to the control, but they more frequently accumulated at temperatures lower than 22 °C (Fig. 1G). This inability to avoid cool temperatures in bishu-1KO and bishu-2KO was rescued by introducing their wild-type alleles (Fig. 1H). These results strengthen the idea that bishu-1 and bishu-2 contribute to cool temperature avoidance. Because a 24 °C versus 20 °C condition yielded the highest PI in control, we performed subsequent two-way choice assays under this condition. Lower PIs in the 24 °C versus 18 °C or 16 °C conditions are likely due to technical reasons. When the early third instar larvae are released at the border between two temperature zones and exposed to 18 °C or lower, their movement can become impaired, causing them to remain in the colder zone

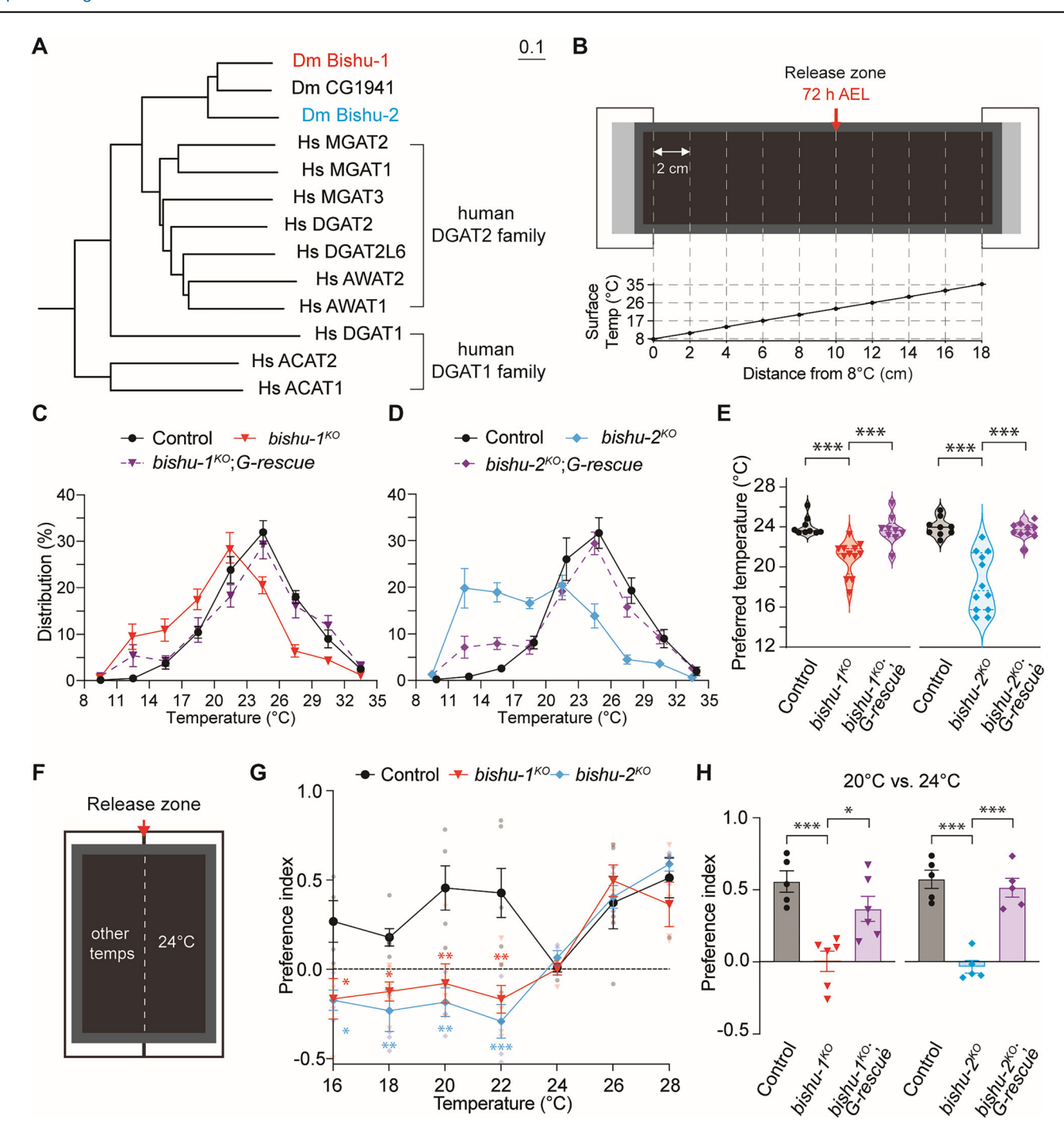


Fig. 1 | bishu-1 and bishu-2 were involved in cool temperature avoidance. A Phylogenetic tree of the *Drosophila* proteins (Dm) CG1941, Bishu-1 and Bishu-2 and the human proteins (Hs) from the DGAT1 family (DGAT1, ACAT1, and ACAT2) and DGAT2 family (DGAT2, DGAT2L6, MGAT1, MGAT2, MGAT3, AWAT1, and AWAT2). The scale bar indicates the p-Distance. B Schematic diagram of the thermal gradient assay. An aluminum testing plate was coated with 2% agarose and placed on two separate aluminum blocks (white boxes), each of which was set up with a distinct temperature using a circulating water bath. Early third instar larvae (72 h AEL) were released at 23 °C (red arrow). After releasing larvae, a glass lid was placed on the testing plate during the assay. The actual temperatures measured on the testing plate with the glass lid are presented. Data are presented as the mean \pm SD (N=3). Error bars are not visible as the variance is smaller than the marker size. C-E Distribution of early third instar larvae (72 h AEL) of each genotype on an 8–35 °C linear gradient (C, D) and the preferred temperature (E). The *G-rescue*

denotes the wild-type of a genomic transgene including CG1941, bishu-1, and bishu-2. C w^{1118} (control), $bishu-1^{KO}$, and $bishu-1^{KO}$; G-rescue (N=9-12 trials). D Control, $bishu-2^{KO}$, and $bishu-2^{KO}$; G-rescue (N=9-12 trials). E The preferred temperature indicates the median staying temperatures, which were calculated using the distribution of larvae in (C (left) and D) (right). F Schematic diagram of the thermal two-way choice assay. An aluminum testing plate was coated with 2% agarose and placed on two adjacent aluminum blocks. Larvae were released at the center zone (red arrow). G Preference indices (PIs) of two-way choice assays between 24 °C versus other temperatures. Larvae of control, $bishu-1^{KO}$, and $bishu-2^{KO}$ (N=4-7 trials). H PIs of two-way choice assays in a 20 °C versus 24 °C condition. Control, $bishu-1^{KO}$, $bishu-1^{KO}$; G-rescue (left); $bishu-2^{KO}$ and $bishu-2^{KO}$; G-rescue (right, N=5-6 trials). The data are presented as the mean \pm SEM except for (B). Each point represents a biological replication. *P < 0.05, *P < 0.01, and **P < 0.001 by one-way ANOVA with Tukey's test (E, H) or Dunnett's test (G). NS denotes not significant.

due to reduced mobility. This "trapping effect" affects the preference index. Supporting this interpretation, control larvae displayed an apparently reduced presence in the $17-20\,^{\circ}\mathrm{C}$ zone compared to the $23-26\,^{\circ}\mathrm{C}$ zone during gradient assays (Fig. 1C, D). This distribution pattern suggests that larvae exhibit an aversion to temperatures below $20\,^{\circ}\mathrm{C}$, actively avoiding migration into these cooler regions.

bishu-1 functions in DOCCs to mediate cool temperature avoidance

To explore the responsible cells for *bishu-1*- and *bishu-2*-dependent thermotaxis, we performed RNAi-mediated knockdown of each gene using the GAL4-UAS expression system. A pan-neuronal driver (*elav-GAL4*)-induced knockdown of *bishu-1* or *bishu-2* resulted in a significant reduction in PI in the 20 °C versus 24 °C condition (Supplementary Fig. 2A), suggesting that these genes function in neurons to discriminate temperatures. Next, we suppressed *bishu-1* or *bishu-2* in sensory neurons expressing thermosensors involved in cool temperature sensation, including TRPL, Inactive (Iav), and IRs^{13,16,38}. Knockdown of *bishu-1* or *bishu-2* in TRPL-expressing neurons did not affect PI (Supplementary Fig. 2B), whereas PI was significantly reduced when *bishu-1* or *bishu-2* was suppressed under the control of *iav-GAL4* (Supplementary Fig. 2C). However, the heterozygous *GAL4* control (*iav-GAL4/+*) displayed variable PIs with a lower average value than other controls, which complicated interpretation of the result.

Previous studies reported that IR25a, IR93a, and IR21a are coexpressed in DOCCs to mediate cool temperature avoidance 16,38. When we suppressed bishu-1 or bishu-2 using IR25a-GAL4, obvious impairments in temperature discrimination were observed between 20 °C and 24 °C (Fig. 2A, B), suggesting possible functions of these genes in DOCCs. Consistent with this idea, the defect in cool temperature avoidance in bishu-1^{KO} was rescued by overexpressing bishu-1 cDNA using IR25a-GAL4 (Fig. 2C). By contrast, overexpressing bishu-2 using IR25a-GAL4 failed to rescue the phenotype in bishu-2^{KO} (Fig. 2D). In addition to thermosensation, IR25a is involved in gustatory sensation in larvae such as denatorium response⁴⁰. To test whether bishu-1 and bishu-2 are involved in other IR25a-dependent sensory processes, we examined their involvement in denatonium avoidance. As reported, IR25a mutant was unable to detect denatonium, whereas neither bishu-1 nor bishu-2 mutants showed defects in denatonium avoidance (Supplementary Fig. 2D). This result suggests a more specific role for bishu genes in thermal sensation rather than general IR25a-dependent sensory pathways. To further explore the functions of bishu-1 and bishu-2 in cool temperature avoidance, we suppressed each gene using DOCC-specific IR21a-GAL4 or R11F02-GAL4^{12,16}. Defects in cool temperature avoidance were observed upon bishu-1 knockdown, but not bishu-2 knockdown, in DOCCs (Fig. 2E, F). R11F02-GAL4-induced overexpression of bishu-1 in the bishu-1^{KO} background sufficiently recovered the preference for 24 °C (Fig. 2G). Moreover, considering the sequence similarity between bishu-1 and the human DGAT2 family, we overexpressed three human genes from this family in bishu-1^{KO} and observed sufficient compensation for the bishu-1^{KO} phenotype by two MGATs, but not by DGAT2 (Fig. 2H). To further validate the role of bishu-1 in DOCCs, we conducted thermal gradient assays corresponding to the knockdown and the rescue experiments in two-way choice assays. The distribution and preferred temperatures demonstrated a reduced cool temperature avoidance when bishu-1 was knocked down using IR21a-GAL4 (Supplementary Fig. 2E, G). When bishu-1 or hMGATs was overexpressed in bishu-1^{KO} using R11F02-GAL4, the thermotactic phenotypes were fully (Supplementary Fig. 2F, G) or partially (Supplementary Fig. 2H-J) restored, respectively. Taken together, these results strongly suggest that bishu-1 and bishu-2 function in multiple but distinct tissues to mediate cool temperature avoidance. Specifically, bishu-1 emerged as a primary contributor in DOCCs with possible MGAT activity.

The absence of bishu-1 affects the cooling response of DOCCs

The functional contribution of *bishu-1* in DOCCs led us to examine whether the gene is expressed in *IR25a* and *IR21a* neurons. We generated a *bishu-1*-P2AQF2 fused line (Supplementary Fig. 3A) and examined the *bishu-1*

expression pattern using QUAS-mCherry as a reporter. In the anterior region of larvae, *IR25a* is expressed in temperature-sensitive neurons, including DOCCs and dorsal organ warm cells (DOWCs)¹⁸. We observed that *bishu-1* expression largely overlapped with *IR25a* neurons (Fig. 3A–C). Among them, three *bishu-1*-expressing neurons were DOCCs because they were co-labeled with *IR21a-GAL4* (Fig. 3D–F and Supplementary Fig. 3B).

To explore the physiological role of bishu-1 in DOCCs, we first examined the morphology of DOCCs in bishu-1^{KO} and observed no obvious changes in the cell bodies and dendritic bulbs, a unique structure in DOCCs¹² (Supplementary Fig. 4). Previous studies reported that cooling responses in DOCCs rely on IR25a and IR21a, and these responses are required for the avoidance of innocuous cool temperatures 16,38. Because bishu-1 was co-expressed with IR25a and IR21a, we performed in vivo Ca²⁺ imaging to evaluate the thermal responsiveness of DOCCs. We expressed GCaMP8m in DOCCs using R11F02-GAL4 and examined DOCCs under the same temperature protocol. Both control and bishu-1^{KO} DOCCs responded to temperature increases and decreases (Fig. 4A-C). However, the cooling-induced Ca²⁺ increase was significantly reduced in bishu-1^{KO} (Fig. 4C-E). The reduction was evident in the cooling-induced peak responses and following sustained phases during cooling stimulation. The defect was restored by overexpressing bishu-1 transcripts in the DOCCs using the R11F02-GAL4 (Fig. 4C-E). To examine the potential effects of Zdrift, we evaluated the magnitude of temperature-induced z-drift in our specific setup by expressing GFP in DOCCs and subjecting these preparations to the same temperature protocol used in Fig. 4C (24-18 °C transitions). This control experiment demonstrated that the temperature fluctuations induced only minor changes in GFP signal intensity when cells remained in focus (Supplementary Fig. 5A, B). Taken together, these results indicate that the loss of bishu-1 affects the cool responsiveness of DOCCs.

In addition to DOCCs, *bishu-1* and *IR25a* co-expressed in multiple cells (Fig. 3A–C). Since *IR25a* mediates warming responses in DOWCs¹⁸, we examined the function of *bishu-1* in DOWCs. We suppressed *bishu-1* in DOWCs with *IR68a-GAL4* and observed a reduced discrimination between 20 °C and 24 °C (Supplementary Fig. 5C). We then conducted in vivo Ca²⁺ imaging in DOWCs. Temperature fluctuation between 24 °C and 18 °C caused a slight but significant reduction in warming-induced Ca²⁺ increase in *bishu-1*^{KO} (Supplementary Fig. 5D–H). When we attempted to rescue this phenotype by overexpressing *bishu-1* transcripts in DOWCs with *IR68a-GAL4*, we observed only a partial restoration of the Ca²⁺ response (Supplementary Fig. 5F–H). These results suggest that the thermal choice defect caused by *bishu-1* knockdown in DOWCs is likely associated with the reduced DOWC responses. However, the incomplete rescue by *bishu-1* overexpression indicates that the precise role of *bishu-1* in DOWCs is more complex and requires further investigation.

bishu-1 regulates Ir25a mRNA levels through the transcription factor broad

A previous study claimed that thermal preference was synchronized with expression changes in IR25a, IR21a, and IR93a³⁸. Specifically, high or low expression of these receptors was accompanied by avoidance or acceptance of cool temperatures, respectively. Therefore, we examined the transcriptional levels of IR25a, IR21a, and IR93a, which function in DOCCs16,38. We also tested IR68a, which is expressed in DOWCs for warming detection but is absent in DOCCs¹⁸. Because of the difficulty in isolating DOCCs from the dorsal organ ganglion (DOG)⁴¹, we collected the anterior region of larvae where DOCCs are located (Supplementary Fig. 6A) and compared mRNA levels between control and bishu-1^{KO} cells. At the early third instar stage, the mRNA levels of IR25a and IR21a were significantly reduced to approximately 50% of the control level in bishu-1^{KO}, whereas IR93a and IR68a levels were not altered, suggesting that bishu-1 could influence the expression of IRs in DOCCs (Fig. 5A, B). Contrarily, the levels of IR25a and IR21a did not differ between the control and bishu-1KO at the late third instar stage (Supplementary Fig. 6B). When IR25a was overexpressed in bishu-1^{KO} using IR25a-GAL4 or R11F02-GAL4, the behavioral defect in discriminating

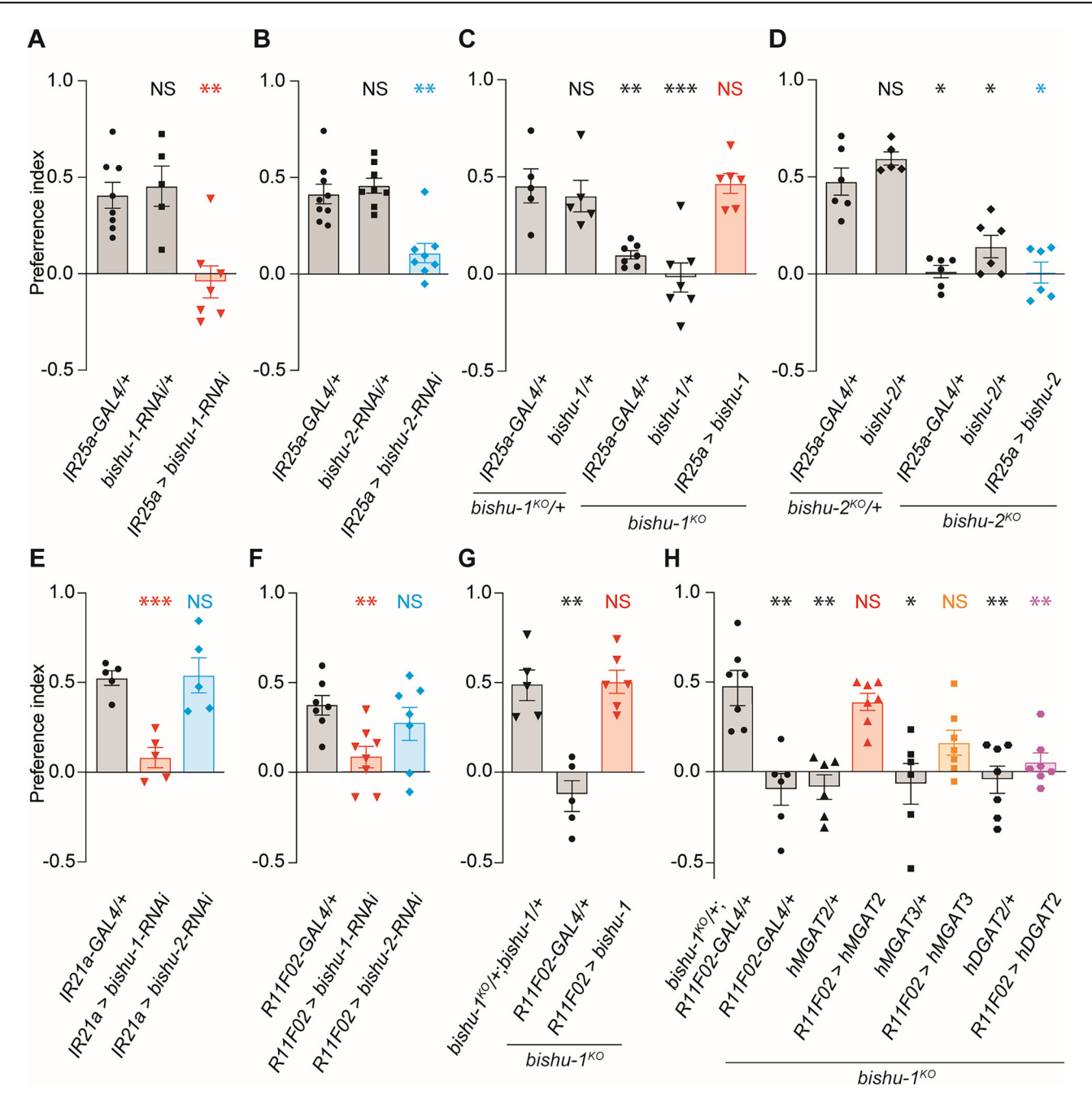


Fig. 2 | bishu-1 functioned in cool temperature avoidance in DOCCs. Preference indices (PIs) of two-way choice assays in a 20 °C versus 24 °C condition with the indicated genotypes. **A**, **B** Knockdown of bishu-1 (**A**) or bishu-2 (**B**) in IR25a-expressing neurons (N = 5-9 trials). **C**, **D** Rescue of bishu-1^{KO} (**C**) or bishu-2^{KO} (**D**) by introducing a wild-type transgene under the control of IR25a-GAL4 (N = 5-7 trials). **E**, **F** Knockdown of bishu-1 or bishu-2 in DOCCs using a specific driver IR21a-GAL4 (**E**) or R11F02-GAL4 (**F**, N = 5-8 trials). **G** Rescue of bishu-1^{KO} by overexpressing

wild-type bishu-1 in DOCCs using R11F02-GAL4 (N=5-6 trials). H Thermal choice of $bishu-1^{KO}$ overexpressing human genes. Transgenes of human MGAT2 (UAS-hMGAT2), MGAT3 (UAS-hMGAT3), and DGAT2 (UAS-hDGAT2) were expressed in $bishu-1^{KO}$ using R11F02-GAL4 (N=5-7 trials). The data are presented as the mean \pm SEM. $^*P < 0.05$, $^*P < 0.01$, and $^**P < 0.001$ by one-way ANOVA with Dunnett's test (\mathbf{A} - \mathbf{C} and \mathbf{E} - \mathbf{H}) or the Kruskal–Wallis test with Steel's test (\mathbf{D}). NS denotes not significant.

between 20 °C and 24 °C was rescued (Fig. 5C). In thermal gradient assays, overexpressing *IR25a* in *bishu-1*^{KO} with *R11F02-GAL4* suppressed the accumulation in cool temperature zones and restored preferred temperature to the control level (Supplementary Fig. 6C, D). In vivo Ca²⁺ imaging results also indicated that *IR25a* overexpression is sufficient to rescue the Ca²⁺ responses of DOCCs during cooling in the absence of *bishu-1* (Fig. 4C–E). In addition, the thermotactic phenotypes of *bishu-1*^{KO} expressing *IR21a* genomic transgene were comparable with *bishu-1*^{KO}/+ and *IR21a* transgene-expressing *bishu-1*^{KO}/+ controls (Fig. 5C and Supplementary Fig. 6E, F). These results suggested that *bishu-1* is required to maintain the

expression of cool temperature-sensitive \it{IR} genes and the responsiveness of DOCCs.

To explore the possible interaction between *bishu-1* and *IR25a*, we sought transcription factors that are predicted to bind to the upstream region of *IR* genes. The database for transcription factor-binding sites (JASPAR 2022) suggested multiple candidates that are common or unique among *IR* genes and *bishu-1*, including six transcription factors upstream of the *IR25a* start codon (Supplementary Fig. 6G, H). Among these candidates, *broad* (*br*) expression was significantly reduced to approximately 50% of the control level, whereas other transcription factors were not suppressed

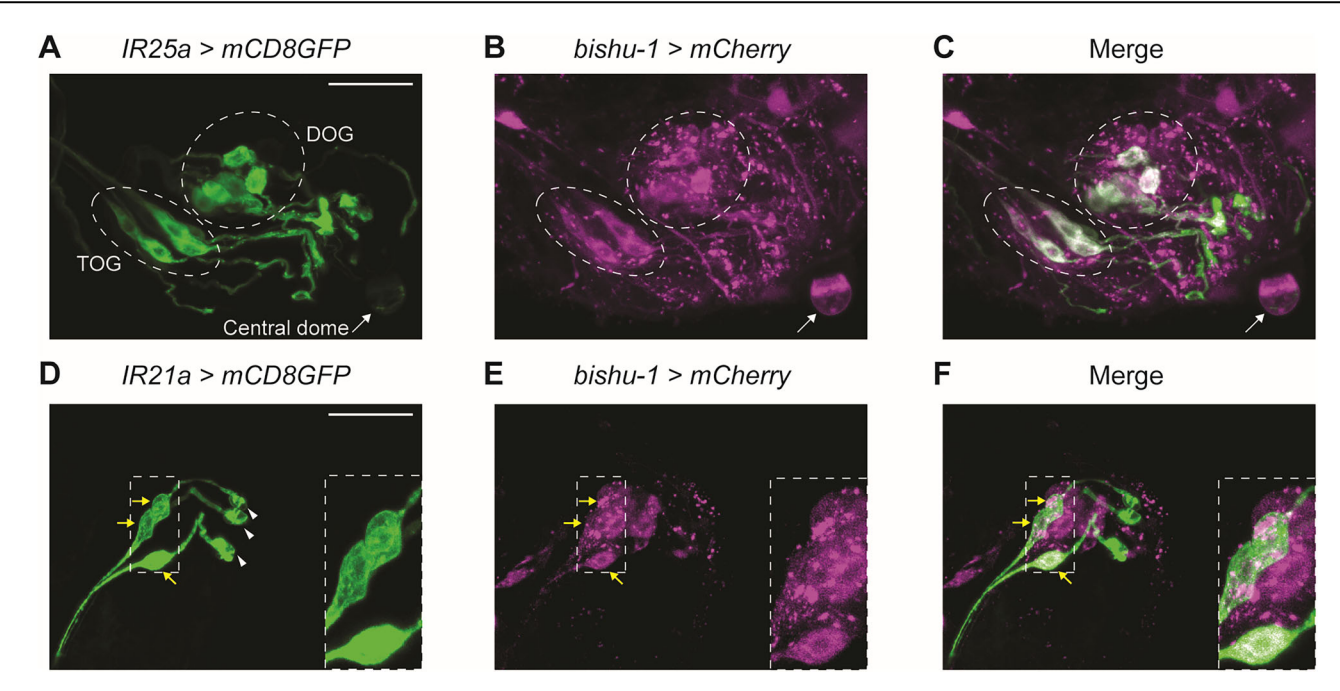


Fig. 3 | bishu-1 was expressed in IR25a- and IR21a-expressing neurons. A–C Representative images of bishu-1 and IR25a reporter expression in the anterior region of larvae. IR25a-GAL4 (A, IR25a-GAL4/+;UAS-40×GFP/+), bishu-1-P2AQF2 (B, $10\times QUAS-6\times mCherry/+$;bishu-1-P2AQF2/+), and the merged image (C). Dashed circles indicate the DOG and terminal organ ganglion (TOG), whereas the right arrow indicates the central dome, a perforated cuticular structure at the tip of the head (A–C). D–F Representative images of bishu-1 and IR21a reporter

expression in the anterior region of larvae. IR21a-GAL4 (D, IR21a-GAL4/+;UAS- $40\times GFP$ /+), bishu-1-P2AQF2 (E, $10\times QUAS$ - $6\times mCherry$ /+;bishu-1-P2AQF2/+), and the merged image (F). Yellow arrows and white arrowheads denote the cell bodies (D–F) and dendritic bulbs of DOCCs (D), respectively. The positions of the cell bodies of DOCCs (D–F) were highlighted as magnified insets in dashed boxes. In all images, the right side is the anterior end. Scale bars in A and D indicate 20 μ m. The expression pattern was investigated in three or more animals.

(Fig. 5D and Supplementary Fig. 6I). br has been reported to have at least four functional splicing variants (Supplementary Fig. 7A)⁴², and br-Z2, br-Z3, and br-Z4, but not br-Z1, were significantly suppressed in bishu- 1^{KO} (Fig. 5D). Consistent with this, knockdown of br in DOCCs using R11F02-GAL4 resulted in no discrimination between 20 °C and 24 °C in larvae (Fig. 5E). Furthermore, the behavioral defect in bishu- 1^{KO} was rescued by overexpression of br-Z4, but not br-Z1, br-Z2, or br-Z3, both in two-way choice and gradient assays (Fig. 5F and Supplementary Fig. 7B–D). In vivo Ca²⁺ imaging results also indicated that br-Z4 overexpression is sufficient to rescue the Ca²⁺ responses of DOCCs during cooling in the absence of bishu-1 (Fig. 4C–E). Collectively, these results suggested that the bishu-1-dependent transcriptional regulation of IR25a and br contributes to the ability of DOCCs to regulate cooling temperature avoidance in larvae.

Discussion

Our study provides evidence that the peripheral sensory process is maintained by the lipid metabolizing enzymes with putative MGAT activity, and one enzyme regulates the transcriptional level of the thermosensors IR25a and IR21a in DOCCs. Lipid metabolism is fundamental for many cellular functions, ranging from cell membrane properties and lipid composition to intra-/intercellular signaling and energy storage^{43,44}. In particular, DAG and its metabolites play key roles in regulating the activation of sensors and other membrane molecules, thereby affecting cellular and physiological responses^{27,45–47}. In addition, a recent study clarified that *fa2h*, which encodes a fatty acid 2-hydroxylase that maintains the cool temperature responsiveness of DOCCs in *Drosophila* larvae by regulating membrane rigidity through 2-OH sphingolipid production²². Apart from these examples, our study revealed an unexpected link between DAG biosynthesis enzymes and the regulation of thermosensor expression, which contributes to the avoidance of cool temperatures in animals. Drosophila larvae exhibit a developmental switch in their thermal preference from warm (24 °C) to cool temperature (18 °C), and this switch depends on the rhodopsin signaling cascade in TRPA1-expressing neurons^{5,7} and IRs in DOCCs³⁸. The latter

case involves the association of the thermal preference switch with the reduced expression of multiple *IR* genes at late larval stages³⁸. Whether the development-dependent regulation of *IR* expression is mediated by *bishu-1* requires further study.

We identified the transcription factor, which could act as one of the transcription factors for the proper expression of IR25a (Fig. 5). The roles of br in metamorphosis and development have been well characterized⁴⁸, and multiple isoforms are expressed during central nervous system development⁴⁹. However, the regulatory mechanisms of *br* expression have not been clarified. Based on previous research and the current study, we can speculate several possible mechanistic links between br and bishu-1. For example, br is downregulated by harmful stimuli such as hypoxic stress⁵⁰ and toxic drug treatment⁵¹. Because bishu-1 contributes to lipid droplet formation through its MGAT activity^{52,53} and lipid droplets have been suggested to have a protective role against oxidative stress⁵⁴, it can be hypothesized that a reduction in lipid droplet content attributable to the absence of bishu-1 increases oxidative stress, leading to a reduction in br expression. Another possible interaction between bishu-1 and br might exist in some signaling cascades. In Drosophila larval brain neural stem cells, atypical PKC directly phosphorylates zinc-finger transcription factor (zif), thereby decreasing its activity by excluding it from the nucleus⁵⁵, whereas an interaction between br and zif was found in Drosophila transcription factor interactome analysis⁵⁶. Additionally, PKC supports the nuclear entry of br via RACK1 in silk moths⁵⁷. Because MGATs can derive the specific DAG isomer, 1,2-sn DAG, to activate PKCs^{58,59}, bishu-1-dependent DAG production and PKC activation might control br-zif formation in DOCCs. Furthermore, br mediates the ecdysone signaling pathway^{60,61}, which regulates the dendritic pruning of Drosophila peripheral neurons during metamorphosis through AMPK-dependent gene regulation⁶². Another study reported that bishu-1 has an indirect interaction with the AMPK pathway in skeletal muscle performance⁶³. Therefore, it could be intriguing to examine the function of bishu-1 and br in the AMPK signaling pathway during DOCC development.

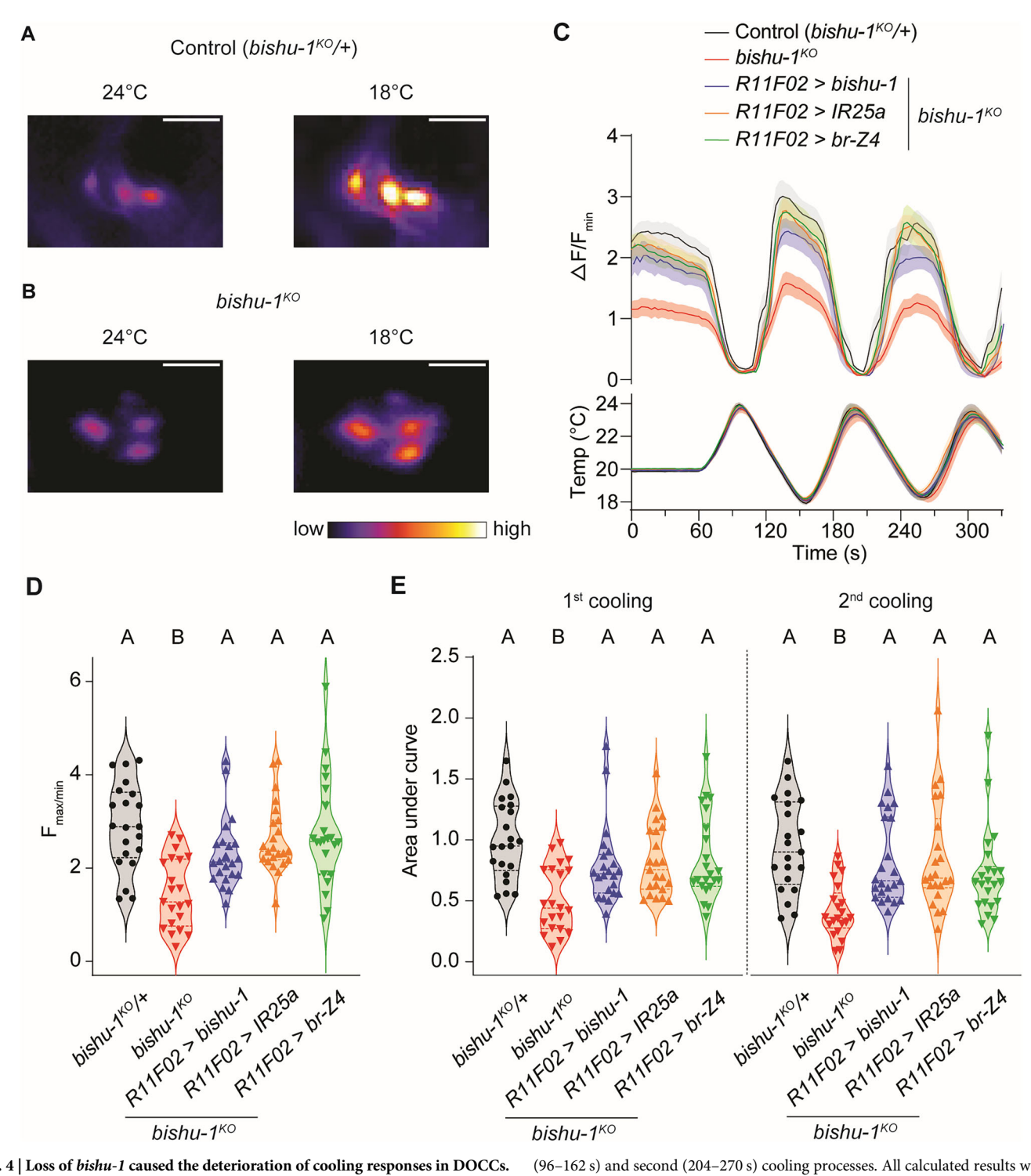


Fig. 4 | Loss of bishu-1 caused the deterioration of cooling responses in DOCCs. A, B Representative GCaMP8m responses of DOCCs in the heterozygous control (bishu- $1^{KO}/+$, A) and bishu- 1^{KO} (B) at 18 °C or 24 °C. GCaMP8m was expressed in DOCCs using R11F02-GAL4. Scale bars indicate 20 µm. C GCaMP8m responses ($\Delta F/F_{\min}$) in bishu- $1^{KO}/+$ (black), bishu- 1^{KO} (red), and bishu- 1^{KO} overexpressing bishu-1 (blue), IR25a (orange), and br-Z4 (green) in DOCCs. F_{\min} was taken between 60 s and 300 s. D Quantification of the averaged maximum Ca²⁺ responses of two cooling processes in (C). E Quantification of the area under the curve during the first

(96–162 s) and second (204–270 s) cooling processes. All calculated results were normalized to the first cooling response of $bishu-1^{KO}/+$. The data are presented as the mean \pm SEM. $bishu-1^{KO}/+$: N=21 cells (from 10 animals); $bishu-1^{KO}$: N=21 cells (from 11 animals); $bishu-1^{KO}$; $R11F02 > bishu-1^{KO}$; R11F02 > IR25a: N=22 cells (from 13 animals); $bishu-1^{KO}$; R11F02 > IR25a: R11F02 > IR25a

We observed reduced responses of DOCCs to cooling stimulation in bishu-1^{KO} (Fig. 4), which was fully rescued by IR25a overexpression. Additionally, while the expression level of DOWCs-specific receptor IR68a remained unchanged in bishu-1^{KO} (Fig. 5), the absence of bishu-1 induced the decline of warming responses in DOWCs, possibly due to reduced IR25a

expression (Supplementary Fig. 5). These results suggest that *IR25a* expression level is critical for the thermal sensitivity of DOCCs/DOWCs at the early third instar stage. In adult *Drosophila*, *IRs* including *IR25a* are required for the morphological arrangement of cooling cells, which have corresponding functions to DOCCs in larvae. However, we found no clear

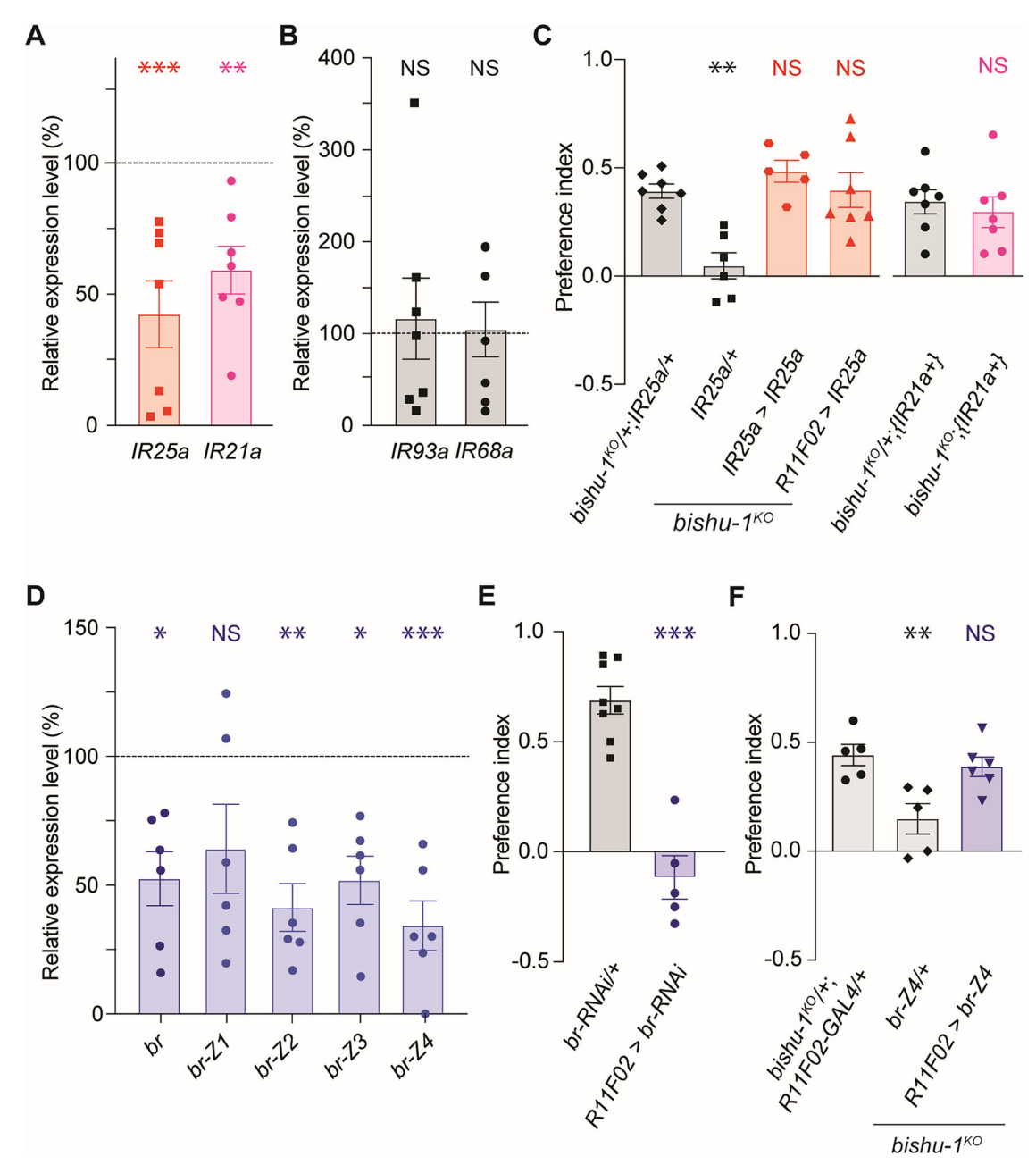


Fig. 5 | bishu-1 regulated IR25a levels through the transcription factor br. A, B The relative expression of IR25a and IR21a (A); IR93a and IR68a (B) in the anterior region of bishu-1^{KO} (N=7 trials). The expression of each gene was normalized to that of the control (w^{1118} , 100%, N=7 trials). C Rescue of bishu-1^{KO} in two-way choice assays in the 20 °C versus 24 °C condition. Overexpression of IR25a in IR25a-expressing neurons (IR25a-GAL4), or DOCCs (R11F02-GAL4), and an insertion of IR21a genomic transgene were examined (N=5-7 trials). D The relative expression of all isoforms (br) or a specific isoform (br-Z1, Z2, Z3, and Z4) in the

anterior region of *bishu-1*^{KO} (N=6 trials). The expression of each gene was normalized to that of the control (N=6 trials). **E** The effect of br knockdown in DOCCs using R11F02-GAL4 in the two-way choice assay in the 20 °C versus 24 °C condition (N=5-8 trials). **F** Rescue of bishu-1^{KO} in the two-way choice assay in the 20 °C versus 24 °C condition by overexpressing br-Z4 in DOCCs (R11F02-GAL4, N=5-6 trials). The data are presented as the mean \pm SEM. *P<0.05, **P<0.01, and ***P<0.001 by one-way ANOVA with Dunnett's test. NS denotes not significant. (**A**, **B**, **D**).

morphological differences in DOCCs between control and bishu-1^{KO} larvae at early third instar stage (Supplementary Fig. 4). On the other hand, at late third instar stage, despite no further reduction in IR expression (Supplementary Fig. 6), bishu-1 continues to affect thermal preference (Supplementary Fig. 1), suggesting additional mechanisms. Given that br (which interacts with bishu-1) plays critical roles in neural development⁶⁴, we hypothesize that these later-stage effects might involve developmental processes in the DOCCs through the bishu-1-br axis, independent of IR expression.

We observed that introducing either IR25a or IR21a expression restored the thermal preference in the absence of bishu-1 (Fig. 5 and

Supplementary Fig. 6). A previous study suggests that *IR21a* expression level is associated with *IR25a*⁶⁵. Based on this relationship, we hypothesize that overexpressing *IR25a* in *bishu-1*^{KO} larvae may indirectly upregulate *IR21a* expression, thereby restoring cool temperature responses and avoidance behavior. This potential regulatory relationship could explain why *IR25a* overexpression is sufficient for rescue even when baseline *IR21a* expression is reduced in *bishu-1*^{KO}. However, the precise mechanisms remain to be fully elucidated. Specifically, we don't yet understand how whole-body *IR21a* transgene expression recovers the *bishu-1* thermotactic phenotype, or whether *IR25a* and *IR21a* reciprocally regulate each other's expression. Future studies will aim to clarify these interactions between *bishu-1*, *br*, and *IRs*.

bishu-1 has been predicted to be a DGAT based on its sequence alignment and involvement in lipid droplet formation ⁵². However, given that the amino acid identity of bishu-1 with human MGAT2 (39.5%) and MGAT3 (38.1%) is higher than that with human DGAT2 (30.7%), its molecular function as a DGAT has not been confirmed ^{52,66}. Our results demonstrated that multiple human MGATs, but not DGAT2, compensated for the physiological function of bishu-1 (Fig. 2), supporting the idea that bishu-1 functions as an MGAT. As discussed above, bishu-1 possibly regulates the expression of br and IR genes through lipid droplet formation and/or DAG production. Further biochemical analyses will clarify the molecular function of bishu-1 and the downstream mechanisms for gene regulation.

bishu-1 forms a tandem structure together with bishu-2 and CG1941 in the genome (Supplementary Fig. 1). A previous study observed that while the transcriptional expression in the tandem is interdependent, these lipid enzymes with close molecular function display independent roles⁶⁷. This supports that, although bishu-1, bishu-2, and CG1941 display interactions at a mRNA level (Supplementary Fig. 1), they contributed to thermotaxis distinctively. We also identified bishu-2 as a responsible gene for cool temperature avoidance (Fig. 1). The high amino acid identity between bishu-1 and bishu-2 (67.1%) suggests similar molecular functions. In contrast to bishu-1, bishu-2 did not play a major role in DOCCs (Fig. 2) and functioned in other thermosensitive neurons such as IR25a-positive neurons (excluding IR21a-positive neurons) and chordotonal organs (Supplementary Fig. 2). However, we haven't identified a specific tissue where bishu-2 plays the dominant role. We expect that bishu-1 and bishu-2 play distinctive and comprehensive roles in the thermotaxis of larvae. CG1941 did not contribute to thermotaxis (Supplementary Fig. 1), although it exhibited higher amino acid identity with bishu-1 than bishu-2 (69.6%). Comparing the expression pattern of CG1941 to those of bishu-1 and bishu-2 could provide clues to understand their different physiological functions.

In this study, we demonstrated advantages of using distinct types of temperature assays, two-way choice and gradient assay, to evaluate thermotactic phenotypes. In the two-way choice assay, larvae make binary decisions at temperature border, while in the gradient assay, they navigate and settle within a continuous temperature range, typically forming distribution peaks around preferred temperatures. The accumulation of bishu mutants in cooler regions in the gradient assay raised two possibilities, either lack of cool avoidance or enhanced heat avoidance. By combining the result with their inability to discriminate between 20 °C and 24 °C in the two-way choice assay (while maintaining normal warmth avoidance, Fig. 1), we conclude that these mutants have specific defects in cool temperature sensation rather than enhanced heat avoiding behavior. This conclusion is further supported by the observation that bishu mutants show normal noxious cold avoidance in gradient assays. These results are in line with the observation that bishu-1 functions in DOCCs involved in cool but not noxious cold range.

Taken together, our findings highlight the unpredicted role of *bishu-1* in cool temperature sensation through the regulation of thermosensors and a transcription factor. A number of investigations have revealed the function of *IR* genes in chemical sensation, thermal sensation, and hygrosensation ^{41,68,69}, but little attention has been paid to their regulatory mechanisms. The current study provided novel insight into the functional correlation between lipid metabolism and sensory functions and proved the physiological importance of the coupling of lipid and sensors in appropriate sensory outputs.

Methods

Fly stocks and husbandry

The following strains were obtained from the Bloomington *Drosophila* Stock Center (Bloomington, IN, USA): *bishu-1/2* transgenic BAC line (#90443), *UAS-dicer2* (#24650), *elav-GAL4* (#8760), *iav-GAL4* (#52273), *TRPL-GAL4* (#29134), *IR25a-GAL4* (#41728), *R11F02-GAL4* (#49828), *UAS-hMGAT2* (#82252), *UAS-hMGAT3* (#84925), *UAS-hDGAT2* (#84854), *40×UAS-IVS-mCD8GFP* (#32195), *10×QUAS-6×mCherry*

(#52269), 5×UAS-mCD8::GFP (#5137), 20×UAS-IVS-jGCaMP8m (#92591), UAS-IR25a (#78067), UAS-br-Z1 (#51190), UAS-br-Z3 (#51192), and UAS-br-Z4 (#51193). The following RNAi lines were obtained from the Vienna Drosophila Resource Center (Vienna, Austria): UAS-bishu-1-RNAi (#7942), UAS-bishu-2-RNAi (#108495), and UAS-br-RNAi (#104648). IR21a-GAL4, IR68a-GAL4, UAS-IR25a, and IR21a genomic rescue line were provided by P. Garrity. The following stocks were created in our laboratory: CG1941^{KO}, bishu-1^{KO}, bishu-2^{KO}, UAS-bishu-1, UAS-bishu-2, UAS-br-Z2, and bishu-1-P2AQF2. We used w¹¹¹⁸ as the wild-type control, and all stocks used for behavioral assays were outcrossed with the control line for at least five generations. UAS-dicer2 was combined with all RNAi lines to enhance the efficiency of knockdown.

Flies were reared on glucose–yeast–cornmeal medium [180 g of cornmeal, 100 g of dry brewer's yeast Ebios, 19 g of agar, 250 g of glucose, 24 ml of methyl 4-hydroxybenzoate (10% w/v solution in 70% ethanol), and 8 ml of propionic acid in 2500 ml of reverse osmosis (RO) water]. Flies were raised in vials or bottles in a 25 °C incubator under a 12-h/12-h light/dark cycle.

Phylogenetic comparison of MGATs and DGATs

The amino acid sequences of *Drosophila* and human proteins were obtained GenBank, Drosophila from including melanogaster (NP_001286163), Bishu-1 (NP_610318), and Bishu-2 (NP_610319); human DGAT1 family members [diacylglycerol acyltransferase 1 (DGAT1, NP_036211), acetyl-CoA acetyltransferase 1 (ACAT1, NP_001373606), and ACAT2 (NP_001290182)]; and human DGAT2 family members [DGAT2 (NP_115953), DGAT2L6 (NP_940914), monoacylglycerol acyltransferase 1 (MGAT1, NP_477513), MGAT2 (NP_079374), MGAT3 (NP_835470), acyl-CoA wax alcohol acyltransferase 1 (AWAT1, NP_001013597), and AWAT2 (NP_001002254)]. The phylogenetic tree was constructed by the neighbor-joining algorithm implemented in the MEGA X program⁷⁰ using p-Distance (scale bar).

Thermal preference assays

To prepare synchronized larvae for thermal gradient assays, 12–20 mated females were fed on yeast paste over 2 days and allowed to lay eggs in new food vials in a 3–6-h window. Larvae were raised in the vial until they reach the test stages (second instar, 48 h AEL; early third instar, 72 h AEL; late third instar, 120 h AEL). Larvae collected from the food were separated in 18% (72 and 120 h AEL) or 22% (48 h AEL) sucrose solution in 50-ml tubes (#1342-050S, Watson, Japan) twice, transferred to a 300 μm strainer (#43-50300-01, PluriSelect, Germany), followed by two rounds of washing with RO water. Larvae were kept in a 35 mm dish (#1000-035, Iwaki, Japan) at room temperature for 5–10 min to allow them to recover and subsequently used for the assays.

Thermal gradient assays were conducted following the previously described method^{7,21} with modifications. The test trays were assembled with an aluminum plate $(22.6 \times 6.0 \times 0.1 \text{ cm}^3)$ and black acrylic wall (outer dimension: $20.0 \times 6.0 \text{ cm}^2$, inner dimension: $19.0 \times 5.0 \text{ cm}^2$, 0.5 cm height; Fig. 1B upper). The surface of the aluminum plate was covered with black aluminum tape (#J3270, Nitto, Japan). Trays were coated with 20 ml of 2% agarose. Two rods $(18 \times 0.5 \times 0.5 \text{ cm}^3)$ were placed at the longer edges during agarose solidification to create grooves that minimize larva escape from the agarose after filling with water. The agarose surface was gently scratched and sprayed with water to prevent the gel from drying. Test trays were placed on top of two aluminum blocks separated by 18 cm and individually connected to a circulating water bath (NCB-1210A, Eyela, Japan) to generate a continuous linear temperature gradient from 8 °C to 35 °C (1.5 °C/cm, Fig. 1B lower). The surface temperature of the agarose 0.5 cm from the wall was measured at every 2 cm with a digital thermometer (#MC3000, Chino, Japan).

To initiate the assay, larvae (40–65 individuals) were released in a line at 23 °C (48 and 72 h AEL) or 29 °C (120 h AEL). Each tray was covered with a square glass $(20.0 \times 6.0 \times 0.1 \text{ cm}^3)$ with hydrophilic film (MF-600, Fujifilm Wako Pure Chemical, Japan) on both sides to prevent larval escape, heat

loss, and fogging. Larvae at the second and early third instar stages were allowed to select temperatures on plates for 15 min, whereas tests were conducted for 10 min under LED red light (>600 nm) in a dark box for late third instar larvae. The distribution of larvae was captured by a CCD camera (#FL-CC1218-5MX, Ricoh, Japan) equipped with a 12-mm F1.8 Manual Iris C-Mount lens.

To quantify the distribution of larvae along the thermal gradient, the position of each larva in the image was determined by selecting the center of body using ImageJ (US National Institutes of Health, MD, USA)⁷¹. The staying temperature of each larva was calculated using the following formula: staying temperature (°C) = horizontal distance from the position at 8 °C (cm) \times 1.5 (°C/cm) + 8 °C. The number of larvae in each 2-cm zone (3 °C range) was tabulated in the nine zones and divided by total number of larvae to calculate the proportion. We omitted larvae within 0.5 cm from both sides, those inside the water-filled grooves, those outside of the plates, and immobile larvae in the release zone from the calculation.

Thermal two-way choice assays were conducted on a test plate (outer: $14 \times 10.1 \times 0.9$ cm³; inner: $12.9 \times 8.7 \times 0.8$ cm³) coated with 25 ml of 2% agarose (Fig. 1F). The plate was placed on top of two adjacent aluminum blocks that were separated using a plastic film (approximately 1 mm) as a spacer. The blocks were individually temperature-controlled using a circulating water bath. Agarose surfaces were gently scratched and sprayed with water to prevent gels from drying. The surface temperature on the center of each side of the test plate was measured and confirmed using a thermometer.

Early third instar larvae (72 h AEL, 40–65 larvae) were reared and collected as previously described in thermal gradient assays. They were released in a line at the border between two temperature zones and allowed to explore the tray under dim red LED light in a black acrylic box. After 15 min, the distribution of larvae on the plate was captured by a CCD camera, and the number of larvae in each temperature zone was tabulated (Fig. 1F). PI was calculated using the following formula: (number of larvae at 24 °C — number of larvae at other temperatures)/(total number of larvae on the test tray). Larvae within the release zone (1 cm wide) were not counted in either temperature zone, and those outside the trays were not counted in the calculation.

Confocal imaging

To examine the expression pattern of bishu-1 in the DOG of larvae, we established the bishu-1 QF2 line (bishu-1-P2AQF2) carrying IR25a-GAL4 or IR21a-GAL4 and 10×QUAS-6×mCherry carrying 40×UAS-IVS-mCD8::GFP, and then we crossed the bishu-1 QF2-GAL4 line with the mCherry-GFP line. The anterior region of larvae was dissected in phosphate-buffered saline (PBS) and mounted on a glass slide using 50% glycerol/PBS. GFP and mCherry fluorescence was captured using a confocal laser-scanning microscope (SP8, Leica, Germany) equipped with a HC PLAPO 63×/1.40 OIL CS2 objective lens. Z-sections were taken at 1-μm intervals. Images were analyzed using Leica Application Suite X (LAS X) and ImageJ software⁷¹.

Quantitative PCR

Whole-body sample (8–10 larvae) or dissected anterior regions from approximately 70 early third instar larvae (Supplementary Fig. 5A) were homogenized in ice-cold PBS solution with a pestle. Total RNA was extracted with Sepasol-RNA I Super G (#0937984, Nacalai Tesque, Japan) and treated with Recombinant DNase I (#2270 A, Takara, Japan) for 30 min at 37 °C, followed by denaturation with phenol:chloroform:isoamyl alcohol (25:24:1, #25970-14, Nacalai Tesque). RNA was precipitated with 100% ethanol and CH₃COONa (#06893-24, Nacalai Tesque) by incubating at $-20\,^{\circ}\text{C}$ overnight. After obtaining total RNA, cDNA was synthesized from 2 mg of total RNA using ReverTra Ace qPCR RT Master Mix (#FSQ-201, Toyobo, Japan).

qPCR was performed using Thunderbird Next SYBR qPCR Mix (#QPX-201, Toyobo) and StepOne and QuantStudio3 Real Time PCR Systems (Applied Biosystems, MA, USA). qPCR primers are listed in

Supplementary Table 1. *Ribosomal protein 49 (rp49)* was used as a reference gene. Gene expression was quantified with the $\Delta\Delta$ Ct method, and the expression in mutants was normalized to that of a control sample.

In vivo GCaMP-imaging

In vivo GCaMP imaging was conducted following a previously described method with modifications¹². To measure the calcium responses in DOCCs, UAS-GCaMP8m expression was driven by R11F02-GAL4. Early third instar larvae (72 h AEL) were prepared in the same manner as described for thermal preference assays. The anterior region of one larva was fixed on a 15-mm diameter disc made of silicone (KE-1606, Shin-Etsu, Japan) using insect pins (Austerlitz 0.1 mm, Czech Republic) in Ca²⁺-free HL3 solution contained 70 mM NaCl, 5 mM KCl, 10 mM NaHCO₃, 20 mM MgCl₂, 5 mM HEPES, 115 mM sucrose, and 5 mM trehalose (pH 7.2). DOCCs were imaged using a fluorescent microscope with a 25×/0.95 HC Fluotar water immerse lens (Leica). HL3 solution was perfused at 2.6 ml/min by a peristaltic pump (PSM071AA, Advantec, Japan). The temperature of the perfusate was controlled through an inline temperature controller (SC-20, Warner Instruments, MA, USA). The temperature near the larval sample was monitored using a temperature controller (CL-100, Warner Instruments) equipped with a thermistor probe (TA-29, Warner Instruments). Temperature fluctuation was recorded using AxoScope software (Molecular Devices, CA, USA). The GCaMP signal was captured every 3 s using a DFC9000 sCMOS camera (Leica) connected to the microscope (DM6 B, Leica) and recorded by LAS X (Leica). The fluorescence of images was processed with THUNDER in LAS X for computational clearing and StackReg in ImageJ for image stacks alignment, followed by subsequent analysis and measurement in ImageJ⁷¹. Temperature fluctuations were analyzed using Clampfit 11.2 (Molecular Devices).

To minimize z-drift impact in data analyses, we employed strict selection criteria during analysis, tracking only cells that remained in focus throughout the recording based on their morphological appearance. When we detected apparent changes in focus at any timepoint during an experiment, we excluded those specific cells or the entire sample from further analysis (approximately 15% of sample rejection). The Ca²⁺ responses in DOCCs in focus were assessed by calculating changes in fluorescence intensity using the following formula: $[(F_t - F_{min})/F_{min}]$, where F_t and F_{min} represent the value obtained every 3 s and the minimum response during recording, respectively. The maximum response (F_{max}) in each cooling phase was determined as the highest fluorescence intensity during 60--162~s(first) and 168-270 s (second). The area under the curve in each cooling stage was calculated using a trapezoidal rule $[(F_t + F_{t+1})/2 \times 3 \text{ (sampling)}]$ interval)] during 96-162 (first) and 204-270 s (second) and was normalized to the area under the curve of the first cooling phase in heterozygous controls.

Statistical analysis

All data are presented as the mean \pm standard error of mean (SEM) unless otherwise noted. The number of trials, cells, or animals (N) is indicated in the Figure legends. The normality of distributions was assessed by the Shapiro–Wilk test. For pairwise comparisons, normally distributed samples were analyzed using an unpaired two-tailed Student's t-test, and nonnormally distributed samples were analyzed using the Mann–Whitney U test. For multiple pairwise comparisons, normally distributed samples were analyzed using one-way analysis of variance (ANOVA) with Dunnett's or Tukey's post-hoc test, and non-normally distributed samples were analyzed using the Kruskal–Wallis test with the Steel or Steel–Dwass test. Statistical analyses were performed using Prism 10 (GraphPad, CA, USA) or EZR (version 1.61; Saitama Medical Center, Jichi Medical University, Japan)⁷², which is a graphical user interface for R (The R Foundation for Statistical Computing, Austria). Statistical significance was indicated by P < 0.05.

Reporting summary

Further information on research design is available in the Nature Portfolio Reporting Summary linked to this article.

Data availability

Data supporting the conclusions of this article has been included in the article. Source data underlying main figures are provided in Supplementary Data 1. All other data collected during this study were archived in the FigShare data repository: https://figshare.com/articles/dataset/Raw_Data/28815632.

Received: 18 August 2024; Accepted: 1 May 2025; Published online: 29 May 2025

References

- Li, K. & Gong, Z. Feeling hot and cold: thermal sensation in *Drosophila*. Neurosci. Bull. 33, 317–322 (2017).
- Rohacs, T., Thyagarajan, B. & Lukacs, V. Phospholipase C mediated modulation of TRPV1 channels. *Mol. Neurobiol.* 37, 153–163 (2008).
- Buijs, T. J. & McNaughton, P. A. The role of cold-sensitive ion channels in peripheral thermosensation. Front. Cell Neurosci. 14, 262(2020).
- Buijs, T. J., Vilar, B., Tan, C. H. & McNaughton, P. A. STIM1 and ORAI1 form a novel cold transduction mechanism in sensory and sympathetic neurons. *EMBO J.* 42, e111348 (2023).
- Shen, W. L. et al. Function of rhodopsin in temperature discrimination in *Drosophila*. Science 331, 1333–1336 (2011).
- Perez-Cerezales, S. et al. Involvement of opsins in mammalian sperm thermotaxis. Sci. Rep. 5, 16146 (2015).
- Sokabe, T., Chen, H. C., Luo, J. & Montell, C. A switch in thermal preference in *Drosophila* larvae depends on multiple rhodopsins. *Cell Rep.* 17, 336–344 (2016).
- Ohnishi, K. et al. G protein-coupled receptor-based thermosensation determines temperature acclimatization of *Caenorhabditis elegans*. *Nat. Commun.* 15, 1660 (2024).
- Dillon, M. E., Wang, G. & Huey, R. B. Global metabolic impacts of recent climate warming. *Nature* 467, 704–706 (2010).
- Porcelli, D., Gaston, K. J., Butlin, R. K. & Snook, R. R. Local adaptation of reproductive performance during thermal stress. *J. Evol. Biol.* 30, 422–429 (2017).
- Colinet, H., Sinclair, B. J., Vernon, P. & Renault, D. Insects in fluctuating thermal environments. *Annu. Rev. Entomol.* 60, 123–140 (2015).
- Klein, M. et al. Sensory determinants of behavioral dynamics in *Drosophila* thermotaxis. *Proc. Natl. Acad. Sci. USA* 112, E220–E229 (2015).
- Kwon, Y., Shen, W. L., Shim, H. S. & Montell, C. Fine thermotactic discrimination between the optimal and slightly cooler temperatures via a TRPV channel in chordotonal neurons. *J. Neurosci.* 30, 10465–10471 (2010).
- Ni, L. et al. A gustatory receptor paralogue controls rapid warmth avoidance in *Drosophila*. Nature 500, 580–584 (2013).
- Knecht, Z. A. et al. Distinct combinations of variant ionotropic glutamate receptors mediate thermosensation and hygrosensation in *Drosophila*. *Elife* 5, e17879 (2016).
- 16. Ni, L. et al. The ionotropic receptors IR21a and IR25a mediate cool sensing in *Drosophila*. *Elife* **5**, e13254 (2016).
- Budelli, G. et al. Ionotropic receptors specify the morphogenesis of phasic sensors controlling rapid thermal preference in *Drosophila*. *Neuron* 101, 738–747.e733 (2019).
- Hernandez-Nunez, L. et al. Synchronous and opponent thermosensors use flexible cross-inhibition to orchestrate thermal homeostasis. Sci. Adv. 7, eabg6707 (2021).
- Ciardo, M. G. & Ferrer-Montiel, A. Lipids as central modulators of sensory TRP channels. *Biochim. Biophys. Acta Biomembr.* 1859, 1615–1628 (2017).
- Kwon, Y., Shim, H. S., Wang, X. & Montell, C. Control of thermotactic behavior via coupling of a TRP channel to a phospholipase C signaling cascade. *Nat. Neurosci.* 11, 871–873 (2008).
- Suito, T. et al. Functional expression of Δ12 fatty acid desaturase modulates thermoregulatory behaviour in *Drosophila*. Sci. Rep. 10, 11798 (2020).

- Li, Q., Chen, L., Yang, L. & Zhang, P. FA2H controls cool temperature sensing through modifying membrane sphingolipids in *Drosophila*. *Curr. Biol.* 34, 997–1009,e1006 (2024).
- Li, Q., DeBeaubien, N. A., Sokabe, T. & Montell, C. Temperature and sweet taste integration in *Drosophila*. *Curr. Biol.* 30, 2051–2067.e2055 (2020).
- Brankatschk, M. et al. A temperature-dependent switch in feeding preference improves *Drosophila* development and survival in the cold. *Dev. Cell* 46, 781–793.e784 (2018).
- Leung, H. T. et al. DAG lipase activity is necessary for TRP channel regulation in *Drosophila* photoreceptors. *Neuron* 58, 884–896 (2008).
- Delgado, R. et al. Light-Induced opening of the TRP channel in isolated membrane patches excised from photosensitive microvilli from *Drosophila* photoreceptors. *Neuroscience* 396, 66–72 (2019).
- Sokabe, T. et al. Endocannabinoids produced in photoreceptor cells in response to light activate *Drosophila* TRP channels. *Sci. Signal.* 15, eabl6179 (2022).
- Leung, N. Y. et al. Functions of opsins in *Drosophila* taste. *Curr. Biol.* 1367–1379.e1366 (2020).
- 29. Bravo-Ruiz, I., Medina, M. A. & Martinez-Poveda, B. From food to genes: transcriptional regulation of metabolism by lipids and carbohydrates. *Nutrients* **13** (2021).
- 30. Georgiadi, A. & Kersten, S. Mechanisms of gene regulation by fatty acids. *Adv. Nutr.* **3**, 127–134 (2012).
- Li, R. C. et al. PKCepsilon modulates NF-kappaB and AP-1 via mitogen-activated protein kinases in adult rabbit cardiomyocytes. Am. J. Physiol. Heart Circ. Physiol. 279, H1679–H1689 (2000).
- Aziz, M. H. et al. Protein kinase Cepsilon interacts with signal transducers and activators of transcription 3 (Stat3), phosphorylates Stat3Ser727, and regulates its constitutive activation in prostate cancer. Cancer Res. 67, 8828–8838 (2007).
- Garg, R., Caino, M. C. & Kazanietz, M. G. Regulation of transcriptional networks by PKC isozymes: identification of c-Rel as a key transcription factor for PKC-regulated genes. *PLoS ONE* 8, e67319 (2013).
- Mejhert, N. et al. Partitioning of MLX-family transcription factors to lipid droplets regulates metabolic gene expression. *Mol. Cell* 77, 1251–1264.e1259 (2020).
- Yen, C. L., Stone, S. J., Cases, S., Zhou, P. & Farese, R. V. Jr. Identification of a gene encoding MGAT1, a monoacylglycerol acyltransferase. *Proc. Natl. Acad. Sci. USA* 99, 8512–8517 (2002).
- Cao, J., Lockwood, J., Burn, P. & Shi, Y. Cloning and functional characterization of a mouse intestinal acyl-CoA:monoacylglycerol acyltransferase, MGAT2. J. Biol. Chem. 278, 13860–13866 (2003).
- Cao, J., Cheng, L. & Shi, Y. Catalytic properties of MGAT3, a putative triacylgycerol synthase. *J. Lipid Res.* 48, 583–591 (2007).
- Tyrrell, J. J., Wilbourne, J. T., Omelchenko, A. A., Yoon, J. & Ni, L. Ionotropic receptor-dependent cool cells control the transition of temperature preference in *Drosophila* larvae. *PLoS Genet.* 17, e1009499 (2021).
- Liu, J., Sokabe, T. & Montell, C. A Temperature gradient assay to determine thermal preferences of *Drosophila* larvae. *J. Vis. Exp.* 136, e57963 (2018).
- 40. van Giesen, L. et al. Multimodal stimulus coding by a gustatory sensory neuron in *Drosophila* larvae. *Nat. Commun.* **7**, 10687 (2016).
- 41. Ni, L. The structure and function of ionotropic receptors in *Drosophila*. *Front. Mol. Neurosci.* **13**, 638839 (2021).
- Bayer, C. A., Holley, B. & Fristrom, J. W. A. switch in broad-complex zincfinger isoform expression is regulated posttranscriptionally during the metamorphosis of *Drosophila* imaginal discs. *Dev. Biol.* 177, 1–14 (1996).
- Falomir-Lockhart, L. J., Cavazzutti, G. F., Gimenez, E. & Toscani, A. M. Fatty acid signaling mechanisms in neural cells: fatty acid receptors. Front Cell Neurosci. 13, 162 (2019).
- Samovski, D., Jacome-Sosa, M. & Abumrad, N. A. Fatty acid transport and signaling: mechanisms and physiological implications. *Annu. Rev. Physiol.* 85, 317–337 (2023).

- 45. Delgado, R., Munoz, Y., Pena-Cortes, H., Giavalisco, P. & Bacigalupo, J. Diacylglycerol activates the light-dependent channel TRP in the photosensitive microvilli of *Drosophila melanogaster* photoreceptors. *J. Neurosci.* **34**, 6679–6686 (2014).
- Ma, D. K. et al. Acyl-CoA dehydrogenase drives heat adaptation by sequestering fatty acids. Cell 161, 1152–1163 (2015).
- Casas, J., Meana, C., Lopez-Lopez, J. R., Balsinde, J. & Balboa, M. A. Lipin-1-derived diacylglycerol activates intracellular TRPC3 which is critical for inflammatory signaling. *Cell Mol. Life Sci.* 78, 8243–8260 (2021).
- 48. Belles, X. Insect Metamorphosis: From Natural History to Regulation of Development and Evolution. (Academic Press, 2020).
- Zhou, B., Williams, D. W., Altman, J., Riddiford, L. M. & Truman, J. W. Temporal patterns of broad isoform expression during the development of neuronal lineages in *Drosophila*. *Neural Dev.* 4, 39 (2009).
- Zhou, D. et al. Experimental selection for *Drosophila* survival in extremely low O₂ environment. *PLoS ONE* 2, e490 (2007).
- 51. Stern, S., Fridmann-Sirkis, Y., Braun, E. & Soen, Y. Epigenetically heritable alteration of fly development in response to toxic challenge. *Cell Rep.* **1**, 528–542 (2012).
- 52. Wilfling, F. et al. Triacylglycerol synthesis enzymes mediate lipid droplet growth by relocalizing from the ER to lipid droplets. *Dev. Cell* **24**, 384–399 (2013).
- Olarte, M. J. et al. Determinants of endoplasmic reticulum-to-lipid droplet protein targeting. *Dev. Cell* 54, 471–487.e477 (2020).
- Circu, M. L. & Aw, T. Y. Reactive oxygen species, cellular redox systems, and apoptosis. Free Radic. Biol. Med. 48, 749–762 (2010).
- Chang, K. C. et al. Interplay between the transcription factor Zif and aPKC regulates neuroblast polarity and self-renewal. *Dev. Cell* 19, 778–785 (2010).
- Shokri, L. et al. A comprehensive *Drosophila melanogaster* transcription factor interactome. *Cell Rep.* 27, 955–970.e957 (2019).
- Cheng, D. et al. Nuclear import of transcription factor BR-C is mediated by its interaction with RACK1. PLoS ONE 9, e109111 (2014).
- Eichmann, T. O. & Lass, A. DAG tales: the multiple faces of diacylglycerol–stereochemistry, metabolism, and signaling. *Cell Mol. Life Sci.* 72, 3931–3952 (2015).
- Kolczynska, K., Loza-Valdes, A., Hawro, I. & Sumara, G. Diacylglycerolevoked activation of PKC and PKD isoforms in regulation of glucose and lipid metabolism: a review. *Lipids Health Dis.* 19, 113 (2020).
- Karim, F. D., Guild, G. M. & Thummel, C. S. The *Drosophila* Broad-Complex plays a key role in controlling ecdysone-regulated gene expression at the onset of metamorphosis. *Development* 118, 977–988 (1993).
- Fletcher, J. C. & Thummel, C. S. The ecdysone-inducible Broad-complex and E74 early genes interact to regulate target gene transcription and *Drosophila* metamorphosis. *Genetics* 141, 1025–1035 (1995).
- Marzano, M. et al. AMPK adapts metabolism to developmental energy requirement during dendrite pruning in *Drosophila*. Cell Rep. 37, 110024 (2021).
- Livelo, C. et al. Time-restricted feeding promotes muscle function through purine cycle and AMPK signaling in *Drosophila* obesity models. *Nat. Commun.* 14, 949 (2023).
- Scott, J. A., Williams, D. W. & Truman, J. W. The BTB/POZ zinc finger protein Broad-Z3 promotes dendritic outgrowth during metamorphic remodeling of the peripheral stretch receptor dbd. *Neural Dev.* 6, 39 (2011).
- Vulpe, A., Mohapatra, P. & Menuz, K. Functional characterization of odor responses and gene expression changes in olfactory co-receptor mutants in *Drosophila*. bioRxiv 2021.06.18.449017 (2021).
- Wang, W. et al. Lipid-gene regulatory network reveals coregulations of triacylglycerol with phosphatidylinositol/lysophosphatidylinositol and with hexosyl-ceramide. *Biochim. Biophys. Acta Mol. Cell Biol. Lipids* 1864, 168–180 (2019).

- 67. Loehlin, D. W., Kim, J. Y. & Paster, C. O. A tandem duplication in *Drosophila melanogaster* shows enhanced expression beyond the gene copy number. *Genetics* **220**, iyab231 (2022).
- Rytz, R., Croset, V. & Benton, R. Ionotropic receptors (IRs): chemosensory ionotropic glutamate receptors in *Drosophila* and beyond. *Insect Biochem. Mol. Biol.* 43, 888–897 (2013).
- Rimal, S. & Lee, Y. The multidimensional ionotropic receptors of Drosophila melanogaster. Insect Mol. Biol. 27, 1–7 (2018).
- Kumar, S., Stecher, G., Li, M., Knyaz, C. & Tamura, K. MEGA X: molecular evolutionary genetics analysis across computing platforms. *Mol. Biol. Evol.* 35, 1547–1549 (2018).
- 71. Schneider, C. A., Rasband, W. S. & Eliceiri, K. W. NIH image to ImageJ: 25 years of image analysis. *Nat. Methods* **9**, 671–675 (2012).
- Kanda, Y. Investigation of the freely available easy-to-use software 'EZR' for medical statistics. *Bone Marrow Transpl.* 48, 452–458 (2013).

Acknowledgements

The fly stocks used in this study were obtained from the Bloomington Drosophila Stock Center, and Vienna Drosophila Resource Center. We thank Dr. Paul Garrity (Brandeis University) for providing us fly stocks. We thank lab members Dr. Shoma Sato, Naomi Fukuta, Terumi Hashimoto, Aliyu Mudassir Magaji, and Hinata Yamanaka for supporting fly maintenance. We thank Dr. Shinji Takada (National Institute for Basic Biology, NIBB) and Dr. Minako Suzuki (Kyoto University) for providing the confocal microscopy Leica SP8 and supporting the imaging data collection. We also thank the Optics and Imaging Facility, NIBB Trans-Scale Biology center, for technical support in confocal imaging. We thank Zhenbo Jiang (NIBB) for advising the transcription factor analysis using JASPAR 2022. This work was supported by Grant-in-aid for Scientific research 17H07337, 18K06495 and 21H02531 (for T. Sokabe) from Japan Society for the Promotion of Science (JSPS) and Ministry of Education, Culture, Sports, Science and Technology (MEXT), the Japan Agency for Medical Research and Development (AMED)-PRIME 23gm6510014h0002 (for T. Sokabe), and Takeda Science Foundation (for T. Sokabe).

Author contributions

X.D. contributed to designing, conducting, and analyzing the experiments and preparing the draft and the final version of the manuscript. T. Sokabe contributed to designing and supervising the project and preparing the draft and the final version of the manuscript. T. Suito and M. Tominaga contributed to supervising the project and preparing the final version of the manuscript.

Competing interests

The authors declare no competing interests.

Additional information

Supplementary information The online version contains supplementary material available at https://doi.org/10.1038/s42003-025-08154-0.

Correspondence and requests for materials should be addressed to Takaaki Sokabe.

Peer review information Communications Biology thanks the anonymous reviewers for their contribution to the peer review of this work. Primary Handling Editors: Asuka Takeishi and Benjamin Bessieres. A peer review file is available.

Reprints and permissions information is available at http://www.nature.com/reprints

Publisher's note Springer Nature remains neutral with regard to jurisdictional claims in published maps and institutional affiliations.

Open Access This article is licensed under a Creative Commons Attribution-NonCommercial-NoDerivatives 4.0 International License, which permits any non-commercial use, sharing, distribution and reproduction in any medium or format, as long as you give appropriate credit to the original author(s) and the source, provide a link to the Creative Commons licence, and indicate if you modified the licensed material. You do not have permission under this licence to share adapted material derived from this article or parts of it. The images or other third party material in this article are included in the article's Creative Commons licence, unless indicated otherwise in a credit line to the material. If material is not included in the article's Creative Commons licence and your intended use is not permitted by statutory regulation or exceeds the permitted use, you will need to obtain permission directly from the copyright holder. To view a copy of this licence, visit http://creativecommons.org/licenses/by-nc-nd/4.0/.

© The Author(s) 2025